Appendix: Detailed Wind Farm Model and IEEE 14-bus System

Zilong Gong, Junyu Mao, Adrià Junyent-Ferré, *Senior Member, IEEE*, and Giordano Scarciotti, *Senior Member, IEEE*

NOMENCLATURE

Roman symbols

A	Wind turbine swept surface
C	DC bus capacity
I_t	One-mass wind turbine aggregated inertia
K_{C_p}	Constant tip speed ratio speed control law coefficient
L_l	Inductance of the grid connection impedance
P	Generator pole pairs
Q_s	Generator stator reactive power
R	Wind turbine radius
V_{DC}	DC bus voltage
V_{bus}	Infinite bus voltage
c_p	Aerodynamic power coefficient
f	System frequency
f^r	Rated frequency
r_s	Resistance of a single phase of the stator windings
r_l	Resistance of the grid connection impedance
U_g^r	Rated collection grid voltage
U_w^r	Rated wind turbine output voltage
v_w	Wind speed

Greek symbols

Γ_m	Generator torque
Γ_t	Wind turbine torque
β	Pitch angle
λ_m	Flux linkage per rotating speed unit
ν	Gearbox multiplication ratio
ω_{mn}	Nominal generator speed
ω_r	Generator electrical anglular speed
ω_t	Wind turbine speed
ρ	Air density
τ	Time constant of the pitch angle controller
θ_m	Generator shaft angular position
θ_r	Generator rotor electric angle

Superscripts and Subscripts

$*$	Reference value
abc	Vector of *abc* components
qd	Vector of *qd* components
m	Variable related to the generator shaft
r	Variable related to the generator rotor
s	Variable related to the generator stator
t	Variable related to the turbine
z	Variable related to the grid connection point

Zilong Gong, Junyu Mao, Adrià Junyent-Ferré and Giordano Scarciotti are with the Department of Electrical and Electronic Engineering, Imperial College London, London, SW7 2AZ, UK. {zilong.gong18, junyu.mao18, adria.junyent-ferre, g.scarciotti}@imperial.ac.uk.

A. WIND FARM MODEL

In this section, we provide the full model of the wind turbine used in the simulations. The wind turbine model consists of several sub-blocks. We summarise each block in terms of inputs, outputs and detailed equations. The Park and inverse Park transformation of a rotation angle θ are indicated by $T(\theta)$ and $T^{-1}(\theta)$, respectively.

1) Wind turbine dynamics:
Block inputs: θ_m^*, Γ_m and v_w.
Block outputs: θ_m and ω_m.

$$\begin{aligned}\beta(s) &= \frac{1}{\tau s+1}\theta_m^*(s),\\ c_p(\Lambda,\beta) &= c_1(c_2\frac{1}{\Lambda} - c_3\beta - c_4\beta^{c_5} - c_6)e^{-c_7\frac{1}{\Lambda}},\\ \Gamma_t &= \frac{1}{2}c_p\rho A v_w^3\frac{1}{\omega_t},\\ \dot{\omega}_t &= \frac{1}{I_t}(\Gamma_t + \nu\Gamma_m),\\ \dot{\theta}_m &= \omega_m = \nu\omega_t,\end{aligned} \tag{1}$$

where $[c_1 \cdots c_9]$ are wind turbine characteristic parameters and Λ is defined as $\frac{1}{\Lambda} = \frac{1}{\lambda + c_8\beta} - \frac{c_9}{1+\beta^3}$ with $\lambda = \frac{\omega_t R}{v_w}$.

2) Wind turbine speed controller:
Block input: ω_m.
Block outputs: Γ_m^* and θ_m^*.

$$\begin{aligned}K_{C_p} &= \frac{1}{2}\rho A R^3\frac{c_1(c_2+c_6c_7)^3 e^{-\frac{c_2+c_6c_7}{c_2}}}{c_2^2 c_7^4}\\ \Gamma_m^* &= \frac{1}{\nu^3}K_{C_p}\omega_m^2,\\ \theta_m^*(s) &= \frac{K_p s + K_i}{s}(\omega_m(s) - \omega_{mn}(s)).\end{aligned} \tag{2}$$

3) Generator dynamics:
Block inputs: v_s^{qd} and ω_m.
Block outputs: i_s^{qd}, i_s^{abc} and Γ_m.

$$\begin{aligned}v_s^{qd} &= \begin{bmatrix} r_s & \omega_r L_d \\ -\omega_r L_q & r_s\end{bmatrix} i_s^{qd} + \begin{bmatrix} L_q & 0 \\ 0 & L_d\end{bmatrix}\frac{d}{dt}i_s^{qd} + \lambda_m\omega_r\begin{bmatrix}1\\0\end{bmatrix},\\ \Gamma_m &= \frac{3}{2}P(\lambda_m i_{sq} + (L_d - L_q)i_{sq}i_{sd}),\\ i_s^{abc} &= T^{-1}(\theta_r)i_s^{qd},\end{aligned} \tag{3}$$

4) Generator vector controller:
Block inputs: Γ_m^*, i_s^{abc}, ω_m and θ_m.
Block outputs: v_s^{qd} and v_s^{abc}.

$$
\begin{aligned}
i_s^{qd} &= T(\theta_r) i_s^{qbc} \\
i_{sq}^* &= \frac{2}{3P}\frac{\Gamma_m^*}{\lambda_m}, \\
i_{sd}^* &= \frac{2}{3P}\frac{Q_s^*}{\omega_m \lambda_m}, \\
\hat{v}_{sq} &= \frac{K_{pq}s + K_{iq}}{s}(i_{sq}^* - i_{sq}), \\
\hat{v}_{sd} &= \frac{K_{pd}s + K_{id}}{s}(i_{sd}^* - i_{sd}), \\
v_s^{qd} &= \hat{v}_s^{qd} + \begin{bmatrix} 0 & \omega_r L_d \\ -\omega_r L_q & 0 \end{bmatrix} i_s^{qd} + \lambda_m \omega_r \begin{bmatrix} 1 \\ 0 \end{bmatrix}, \\
v_s^{abc} &= T^{-1}(\theta_r) v_s^{qd}.
\end{aligned} \tag{4}
$$

where $\omega_r = P\omega_m$, $\theta_r = P\theta_m$, $v_s^{qd} = [v_{sq}, v_{sd}]^{\mathrm{T}}$, $\hat{v}_s^{qd} = [\hat{v}_{sq}, \hat{v}_{sd}]^{\mathrm{T}}$ and $i_s^{qd} = [i_{sq}, i_{sd}]^{\mathrm{T}}$.

5) DC bus dynamics:
Block inputs: i_l^{abc}, v_l^{abc}, i_s^{abc} and v_s^{abc}.
Block outputs: V_{DC} and i_{DCm}.

$$
\begin{aligned}
\frac{d}{dt}V_{DC} &= \frac{1}{C}(i_{DCm} - i_{DCl}), \\
\{v_l^{abc}\}^{\mathrm{T}} i_l^{abc} &= V_{DC} i_{DCl}, \\
\{v_s^{abc}\}^{\mathrm{T}} i_s^{abc} &= V_{DC} i_{DCm}.
\end{aligned} \tag{5}
$$

6) Grid side system dynamics:
Block inputs: v_z^{abc} and v_l^{abc}.
Block output: i_l^{abc}.

$$
v_l^{abc} = r_l i_l^{abc} + L_l \frac{d}{dt} i_l^{abc} + v_z^{abc}. \tag{6}
$$

7) Grid side controller:
Block inputs: V_{DC} and i_{DCm}.
Block output: i_{DCl}^*.

$$
i_{DCl}^* = \frac{K_{pg}s + K_{ig}}{s}(V_{DC}^* - V_{DC}) + i_{DCm} \tag{7}
$$

8) Grid current controller
Block inputs: V_{DC}, i_{DCl}^*, v_z^{abc} and i_l^{abc}.
Block output: v_l^{abc}.

$$
\begin{aligned}
i_{lq}^* &= \frac{2}{3}\frac{V_{DC}}{v_{zq}} i_{DCl}^*, \\
i_{ld}^* &= 0, \\
\hat{v}_{lq} &= \frac{K_{pc}s + K_{ic}}{s}(i_{lq}^* - i_{lq}), \\
\hat{v}_{ld} &= \frac{K_{pc}s + K_{ic}}{s}(i_{ld}^* - i_{ld}), \\
v_{lq} &= v_{zq} - 2\pi f i_{ld} L_l - \hat{v}_{lq}, \\
v_{ld} &= 2\pi f i_{lq} L_l - \hat{v}_{ld}, \\
\hat{\omega} &= \frac{s + 0.129}{s} v_{zd}, \\
i_l^{qd} &= T(2\pi f t - \hat{\omega} t) i_l^{abc}, \\
v_l^{qd} &= T(2\pi f t - \hat{\omega} t) v_l^{abc}.
\end{aligned} \tag{8}
$$

where $i_l^{qd} = [i_{lq}, i_{ld}]^{\mathrm{T}}$, $v_l^{qd} = [v_{lq}, v_{ld}]^{\mathrm{T}}$ and $v_z^{qd} = [v_{zq}, v_{zd}]^{\mathrm{T}}$.

B. Wind farm parameters

In this section, we summarise the parameters of the wind farm used in the simulation.

1) Wind turbine: $c_1 = 1$, $c_2 = 39.52$, $c_6 = 2.04$, $c_7 = 14.47$, $c_3 = c_4 = c_5 = c_8 = c_9 = 0$, $R = 40$m, $A = 5,026.5\text{m}^2$, $\rho = 1.225\text{kg/m}^3$, $\nu = 90$, $I_t = 4\text{kg}\cdot\text{km}^2$, $\tau = 0.1$s and $v_w = 7\text{m/s}$.
2) Wind turbine speed controller: $\omega_{mn} = 1,602\text{min}^{-1}$, $K_p = 0.1^\circ \cdot s/\text{rad}$ and $K_i = 0.02^\circ/\text{rad}$.
3) Generator: 2 pairs of poles, $r_s = 15\text{m}\Omega$, $\lambda_m = 2.35\text{V}\cdot\text{s/rad}$, $L_q = 0.12732$mH and $L_d = 0.12764$mH.
4) Generator vector controller: $Q_s^* = 10$VAr, $K_{pq} = 0.0637\text{V/A}$, $K_{iq} = 7.5\text{V}/(\text{A}\cdot\text{s})$, $K_{pd} = 0.0638\text{V/A}$ and $K_{id} = 7.5\text{V}/(\text{A}\cdot\text{s})$.
5) DC bus: $C = 10$mF and $V_{DC}^* = 2.6$kV.
6) Grid side system: $r_l = 20\text{m}\Omega$, $L_l = 1$mH, $U_w^r = 0.97$kV, $U_g^r = 66$kV and $f^r = 50$Hz.
7) Grid side controller: $K_{pg} = 0.6032\text{A/V}$ and $K_{ig} = 14.2122\text{A}/(\text{V}\cdot\text{s})$.
8) Grid current controller: $K_{pc} = 0.2803\text{V/A}$ and $K_{ic} = 10\text{V}/(\text{A}\cdot\text{s})$.

C. IEEE 14-bus system

In this section, we introduce the IEEE 14-bus model. This standard power system consists of 14 buses, 5 generators, 11 loads and 20 transmission lines. The diagram of the IEEE 14-bus model is presented in Fig. 1 [1].

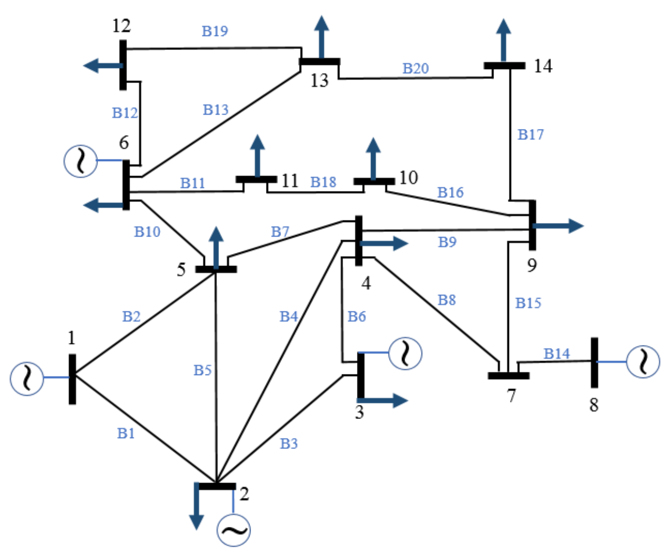

Fig. 1. The diagram of IEEE 14-bus system, indicating generators, loads positions and transmission lines.

D. IEEE 14-bus system parameters

In this section, we summarise the bus and line parameters of the IEEE 14-bus system in Table I and Table II, respectively.

TABLE I
Bus parameters

Bus No.	Generation		Load	
	Real(MW)	Reactive(MVAR)	Real(MW)	Reactive(MVAR)
1	100.0	-16.9	0.0	0.0
2	100.0	42.4	21.7	12.7
3	100.0	23.4	94.2	19.0
4	0.0	0.0	47.8	3.9
5	0.0	0.0	7.6	1.6
6	100.0	12.2	11.2	7.5
7	0.0	0.0	0.0	0.0
8	100.0	17.4	0.0	0.0
9	0.0	0.0	29.5	16.6
10	0.0	0.0	9.0	5.8
11	0.0	0.0	3.5	1.8
12	0.0	0.0	6.1	1.6
13	0.0	0.0	13.5	5.8
14	0.0	0.0	14.9	5.0

TABLE II
Line parameters

Bus No.	Between buses	Line impedance		Half line
		Resistance(pu)	Reactance(pu)	Susceptance(pu)
1	1-2	0.01938	0.05917	0.02640
2	2-3	0.04699	0.19797	0.02190
3	2-4	0.05811	0.17632	0.01870
4	1-5	0.05403	0.22304	0.02460
5	2-5	0.05695	0.17388	0.01700
6	3-4	0.06701	0.17103	0.01730
7	4-5	0.01335	0.04211	0.0064
8	5-6	0.0	0.25202	0.0088
9	4-7	0.0	0.20912	0.0085
10	7-8	0.0	0.17615	0.0090
11	4-9	0.0	0.55618	0.0082
12	7-9	0.0	0.11001	0.0084
13	9-10	0.03181	0.08450	0.0079
14	6-11	0.09498	0.19890	0.0087
15	6-12	0.12291	0.25581	0.0092
16	6-13	0.06615	0.13027	0.0086
17	9-14	0.12711	0.27038	0.0089
18	10-11	0.8205	0.19207	0.0077
19	12-13	0.22092	0.19988	0.0098
20	13-14	0.17093	0.34802	0.0091

E. Robustness analysis of Algorithms

To analyse the robustness of Algorithm 1 and Algorithm 2, we add Gaussian noise to the measurements with the signal-noise-ratio (SNR) of 60dB and 40dB, respectively. We estimate the quantity $C\Pi$ by Algorithm 1 and the quantity ΥB by Algorithm 2 using the data containing the noise. Fig. 2 to Fig. 5 concludes the performances of Algorithm 1 and Algorithm 2 under different levels of noise by showing the regions between the upper and lower envelopes of all obtained magnitude plots of the ROMs obtained for the 20 realisations of the noise. In particular, the red regions refer to the estimation with sufficient measurements ($\widetilde{\nu} = 1000$ or $\widetilde{q} = 1000$), the blue regions refer to the estimation with limited measurements ($\widetilde{\nu} = 30$ or $\widetilde{q} = 1$) and the brown dashed lines represent the ideal estimation (no noise). These figures confirm that the proposed data-driven method is robust with respect to the measurement noise.

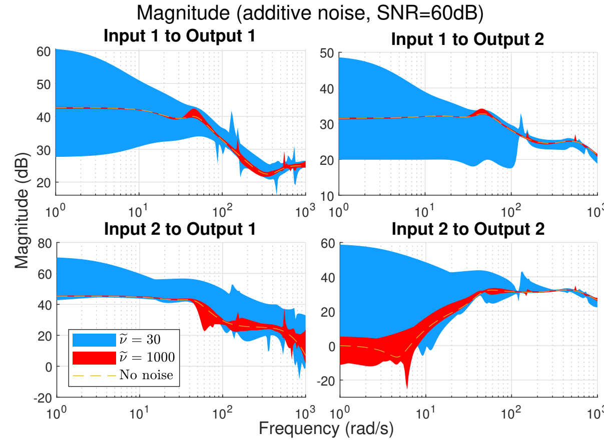

Fig. 2. Magnitude plots of the reduced-order models under 20 realizations of additive Gaussian noise. The red regions, blue regions and brown dashed lines refer to the estimation with 1000 measurements ($\widetilde{\nu} = 1000$), estimation with 30 measurements ($\widetilde{\nu} = 30$) and the ideal estimation (no noise), respectively.

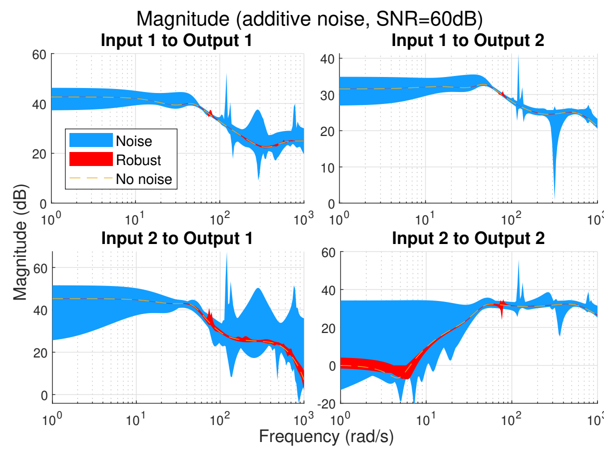

Fig. 3. Magnitude plots of the reduced-order models under 20 realizations of additive Gaussian noise. The red regions, blue regions and brown dashed lines refer to the robust algorithm (Algorithm 2), non-robust method (Theorem 2) and the ideal estimation (no noise), respectively.

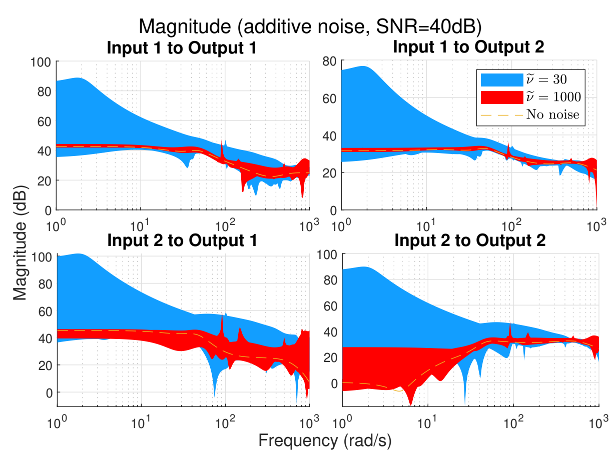

Fig. 4. Magnitude plots of the reduced-order models under 20 realizations of additive Gaussian noise. The red regions, blue regions and brown dashed lines refer to the estimation with 1000 measurements ($\widetilde{\nu} = 1000$), estimation with 30 measurements ($\widetilde{\nu} = 30$) and the ideal estimation (no noise), respectively.

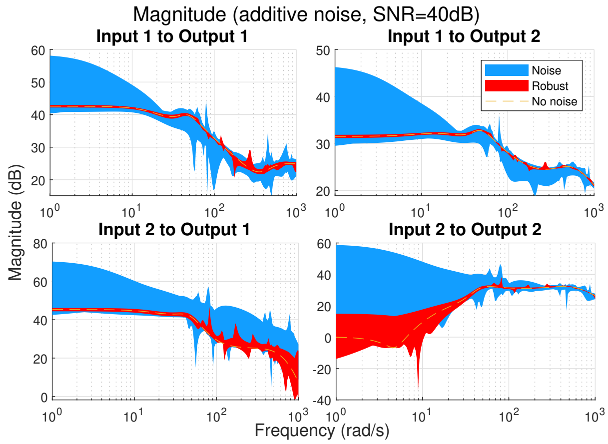

Fig. 5. Magnitude plots of the reduced-order models under 20 realizations of additive Gaussian noise. The red regions, blue regions and brown dashed lines refer to the robust algorithm (Algorithm 2), non-robust method (Theorem 2) and the ideal estimation (no noise), respectively.

F. Code availability

We develop a demo to illustrate the proposed data-driven model order reduction (MOR) method. Provided with a simple benchmark model of the multiple-input-multiple-output (MIMO) systems, the corresponding reduced-order model (ROM) and bode plots are produced by this illustrative demo. For more benchmark models, see [2]. The demo is available at https://github.com/zilong-gong/WindFarmMOR.

References

[1] L. M. Leon, A. S. Bretas, and S. Rivera, "Quadratically constrained quadratic programming formulation of contingency constrained optimal power flow with photovoltaic generation," *Energies*, 2020.

[2] Y. Chahlaoui and P. Van Dooren, "Benchmark examples for model reduction," https://www.slicot.org/20-site/126-benchmark-examples-for-model-reduction, 2002.